2023 62nd IEEE Conference on Decision and Control (CDC)
December 13-15, 2023. Marina Bay Sands, Singapore

Statistical Times Series Based Damage Detection in the Fiber Rope Mooring Lines of the Semi-Submersible OO-STAR Wind Floater

Christos S. Sakaris [1], Rune Schlanbusch [2], Tor A. Nygaard [3], John S. Sakellariou [4] and Murat Tutkun [5]

Abstract— **The Floating Offshore Wind Turbines (FOWTs) based on semi-submersible floaters constitute a popular choice in most markets due to their installation being flexible and in need of low infrastructural requirements. A simple and robust three-legged semi-submersible floater for FOWTs, the OO-STAR wind floater, has been introduced and it can be anchored to the seabed with steel chain mooring lines or hybrid mooring lines - a combination of chains and synthetic fiber ropes. The fiber rope mooring lines present a number of advantages thus leading to a lighter and less costly mooring system. These lines are important for the FOWT's integrity as their loss can lead to the change of the floater's position, a damaged power cable, a possible collision with other infrastructure and high maintenance costs. This why an early detection of damages in the mooring system is crucial. In this study, damage detection in the main part of fiber rope mooring lines of semi-submersible based FOWTs is investigated for the first time. In particular, the OO-STAR floater based FOWT is considered. Two Statistical Time Series based detection methods, the Multiple Model-AutoRegressive (MM-AR) method and the Functional Model Based Method (FMBM) are used and compared. The MM-AR is based on multiple AR models whereas the FMBM on a single Functional Model, for the description of the healthy FOWT's dynamics under varying environmental conditions. The results based on seven healthy and eight damage cases under varying wind speed and wave height show that the two methods are able to achieve damage detection in fiber rope mooring lines without any false alarm or missed damage despite of damages having small effects on the FOWT's dynamics and the fiber ropes presenting a non-linear behaviour.**

I. INTRODUCTION

Currently, three different types of floaters are used in Floating Offshore Wind Turbines (FOWTs): i) spar floaters, ii) semi-submersible floaters and iii) tension leg floaters. Each of the three types has it's strengths and weaknesses. However, the semi-submersible floaters are a popular choice for development in most markets due to the lower infrastructural requirements for their flexible installation which can take place at site locations of any water depth. They deliver the lowest installation costs among the three types due to a number of advantages during their installation such as the capability of full assembling onshore or at quayside, the limited requirement of naval vessels and the tolerance of harsh marine conditions [1].

The semi-submersible floaters are anchored to the seabed with catenary or semi-taut mooring lines which can be steel wires, steel chains or hybrid lines with a combination of chains and synthetic fiber ropes. The fiber ropes present a number of advantages such as being lightweight, reducing the mooring line length and having higher endurance in fatigue and corrosion than chains. As a result, their use for mooring contributes to a lighter and less costly mooring system [1], [2]. However, fiber ropes are non-linear materials with more complex behaviour than steel chains and with responses whose prediction being complicated. Additionally, they are vulnerable to sharp objects and they may require length adjustments and re-tensioning [1], [3], [4].

Nowadays, there is a number of operational semi-submersible floater based FOWTs connected to the electrical grid [5]. These are the FOWTs based on the WindFloat floater in two floating wind farms the WindFloat Atlantic farm in Portugal [1], [2], [6] and the Kincardine farm in Scotland [2], [6] and six single FOWTs based on the VolturnUS floater in USA [1], [7], the Floatgen [8] and Eolink floaters [9] in France, the DemoSATH floater in Spain [10], the TetraSpar floater in Norway [11] and the Sanxia Yinling floater in China [2], [12]. Chain mooring lines alone are used in three of the semi-submersible floaters [6], [7], [13] and a combination of steel wires and chain mooring lines in the Sanxia Yinling floater [2] whereas hybrid mooring lines are used in the WindFloat Atlantic farm and the Floatgen, Eolink and DemoSATH floaters [1], [2], [8], [9], [14]. A semi-taut mooring system is used in the Floatgen and Eolink floaters [2], [9] and a catenary mooring system is used in the rest of the semi-submersible floaters [2], [7], [14].

However, the research on improved concepts of semi-submersible floaters for FOWTs continues and a simple and robust floater, the OO-STAR wind floater, has been designed by the company Dr.techn. Olav Olsen AS (DOOA). The OO-STAR floater consists of a three-legged star-shaped pontoon, a slab below the pontoon, four columns on the pontoon and it is anchored to the seabed with catenary chain mooring lines. This concept has been studied extensively in the context of the LIFES 50+ [15] and FLAGSHIP [16] projects. The current owner of the concept is the company Bouygues Travaux Publics [17]. In the current study, the OO-STAR floater is examined with semi-taut hybrid mooring lines.

The mooring lines are an important component for the integrity of a semi-submersible floater based FOWT and the

[1]Christos S. Sakaris is with the Norwegian Research Centre - NORCE AS, Technology Department, Jon Lilletuns vei 9 H, 3. et, 4879 Grimstad, Norway csak@norceresearch.no

[2]Rune Schlanbusch is with the Norwegian Research Centre - NORCE AS, Technology Department, Jon Lilletuns vei 9 H, 3. et, 4879 Grimstad, Norway rusc@norceresearch.no

[3]Tor A. Nygaard is with the Institute for Energy Technology, 2008, Kjeller, Norway Tor.Anders.Nygaard@ife.no

[4]John S. Sakellariou is with the Department of Mechanical Engineering & Aeronautics, University of Patras, Patras, Greece sakj@mech.upatras.gr

[5]Murat Tutkun is with the Institute for Energy Technology, 2008, Kjeller, Norway Murat.Tutkun@ife.no

most common damage mechanism in them is fatigue [1], [3]. An undetected damage can lead to increased tension in the mooring lines, change of the floater's position, a damaged power cable, a possible collision to other infrastructure and high maintenance costs. Moreover, the access to the underwater mooring lines via an remote operating vehicle is very costly and the FOWT may not be always reachable due to bad weather. Thus, an early detection of damages in such components through an automated and remote method is necessary. However, damage detection in the mooring lines of semi-submersible floater based FOWTs has been investigated in a very limited degree under varying environmental conditions (ECs) [18], [19]. Chain catenary mooring lines [20] have been examined in [18] with damages considered in the lines, whereas hybrid semi-taut mooring lines [21], [22] have been examined in [19] with damages considered only at the mooring connections (fairleads) and the anchor. The two employed methods are based on data-based models (developed with acquired signals from the structure) such as Power Spectral Density (PSD) [19] and Neural Network [18]. In one of the employed methods [19], however the use of varying ECs in the baseline phase is not clear, as well as the method's effectiveness has been examined for only damage scenarios in the inspection (real time) phase and thus with no results on the method's false alarm rate. In addition, damage detection in the hybrid mooring lines of a semi-submersible floater based FOWT such as the OO-STAR floater based FOWT remains uninvestigated.

In the present study, damage detection in the main part of fiber rope mooring lines of semi-submersible floater based FOWTs is investigated for the first time. In particular, the OO-STAR floater based FOWT is considered. Additionally, this is the first study where the semi-submersible OO-STAR floater is considered in relation to damage detection. Two Statistical Time Series (STS) methods, the Multiple Model-AutoRegressive (MM-AR) method [23] and the FMBM [24], are used and compared in the investigation. The time-domain Finite Element Model (FEM) of a FOWT based on the OO-STAR floater is used for the generation of acceleration signals for the considered healthy and damaged fiber rope mooring line under varying mean wind speed (MWS) and significant wave height (SWH). The considered damages correspond to stiffness reduction at different locations in the fiber rope mooring line and of different magnitudes.

II. The OO-STAR Wind Floater Based FOWT and the Simulations

A. The OO-STAR wind floater based FOWT

In the current study, a 10 MW FOWT supported by the OO-STAR wind floater is examined. The 10 MW wind turbine generator is designed by the Danish Technical University and the OO-STAR floater consists of a three-legged star-shaped pontoon, a slab attached to the bottom of the pontoon and four columns, a central column and three outer columns, mounted on the pontoon [15], [16]. The floater is anchored to the seabed with three semi-taut hybrid mooring lines, with each line attached to an outer column. Each line is made of

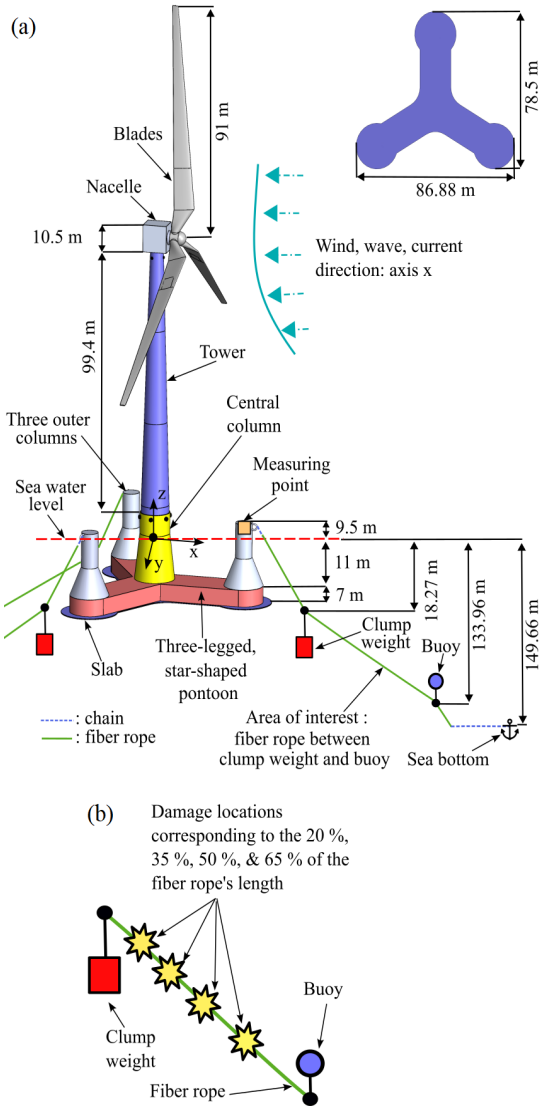

Fig. 1. (a) The OO-STAR wind floater based FOWT with the position of the measuring point and (b) the considered damages

fiber rope and chain and includes a clump weight and a buoy (see Fig. 1(a)). The length of the whole mooring line is 800 m whereas the length and the diameter of the fiber mooring line are 740 m and 25.2 m correspondingly.

The pontoon legs provide structural support for the columns, weight stability, damping/added mass and temporary buoyancy for onshore assembly. The OO-STAR floater can support 12-15 MW wind turbine generators (studies are conducted for 20 MW) under harsh environmental conditions, it can float with very small draft and it doesn't require deep waters at the assembly site. It's material can be steel, concrete or a combination of the two. In the current study, only concrete is considered. The use of post-tensioned concrete as the main material provides a number of advantages such as long design life, less sensitiveness to fatigue and minimum required maintenance. The tower is made of steel, the nacelle of cast iron and the blades of glass fiber reinforced composites. The access to the fairleads is easy as they are above water [16], [17], [25].

B. Simulations and damages

The varying ECs in this study are the MWS and SWH and Table I presents the seven pairs of MWSs / SWHs under which healthy and various damage cases are examined. The considered damage mechanism in the fiber rope is fatigue and it is simulated in each examined damage state via a stiffness reduction of a specific magnitude (%) at a specific location between the clump weight and the buoy of the mooring line (length 580 m). The examined damage magnitudes correspond to 14 %, 27 %, 44 % and 62 % stiffness reduction, whereas the considered damage locations correspond to 20 %, 35 %, 50 % and 64 % of the examined fiber rope's length starting from the clump weight (see Fig. 1(b)). The stiffness reductions are randomly selected for covering damages of higher, middle and low magnitude. As the SWH depends on the MWS, each healthy case is represented by F^{w} with w stating the MWS and each examined damage case by $F^{w}_{m,q}$ with m stating the damage magnitude and q the damage location.

TABLE I
THE CONSIDERED MEAN WIND SPEEDS (MWSS) AND THE CORRESPONDING SIGNIFICANT WAVE HEIGHTS (SWHS) AND PEAK PERIODS (PPS)

MWS (m/s)	10	11.7	12	14.8	16	17.3	18
SWH (m)	2.39	2.74	2.8	3.5	3.85	4.24	4.47
PP (s)	9.39	9.65	9.7	10.2	10.44	10.72	10.97

The FEM of the OO-STAR floater based FOWT has been created jointly by DOOA and the Institute for Energy Technology (IFE) through the aero-hydro-servo-elastic simulation tool 3DFloat [26]. 3DFloat is tailored for large motions, nonlinearities and full coupling between loads, elastic motions and control system. Each time step is solved simultaneously in one FEM with flexible elements from anchor point to wind turbine blade tip [26]. The softness of the mooring system is partly due to the flexibility of the polyester rope and partly by geometric stiffness (catenary effect) provided by the clump weight and buoy. This non-linear effect is described by the Finite-Element corotated approach, where the matrices are updated according to the element orientations for each time step [27].

The FEM with 2706 degrees of freedom and a time step of 0.01 s, is used by IFE for simulations under healthy and damage states. In accordance to the considered MWS, SWH, peak period and turbulence intensity in the simulations, the wind is generated via the Kaimal spectrum [28, p. 30] whereas the irregular waves are generated via the JONSWAP spectrum [29, pp. 106-110]. The surface current of speed 1 m/s and the wind/waves are applied at the same direction (Figure 1(a)).

TABLE II
DETAILS OF THE SIMULATIONS AND THE SIGNALS

Structural state	No. of simulations - Baseline phase	No. of simulations - Inspection phase
Healthy	7 (one per healthy case*)	7 (one per healthy case*)
Damaged	-	12 (one per damage case**)

*Healthy cas.: F^{10}, $F^{11.7}$, F^{12}, $F^{14.8}$, F^{16}, $F^{17.3}$, F^{18}
**Damage cas.: $F^{11.7}_{14,20}$,$F^{11.7}_{44,50}$,$F^{11.7}_{27,65}$,$F^{11.7}_{62,20}$,$F^{14.8}_{14,20}$,$F^{14.8}_{27,35}$,$F^{14.8}_{44,50}$,$F^{14.8}_{62,20}$, $F^{17.3}_{14,20}$,$F^{17.3}_{14,35}$,$F^{17.3}_{27,65}$,$F^{17.3}_{44,65}$
Sampling frequency: f_s = 10 Hz, Signal bandwidth: [0 − 5] Hz
Signal length: N=20 000 samples (≈ 1000 seconds)

In every conducted simulation, an axis z based acceleration signal is generated based on a measuring point at the fairlead in one of three outer columns (see Fig. 1(a)). 14 different simulations (seven per baseline / inspection phase) are performed for the healthy state under seven WSs, while eight for the damaged FOWT under the same WSs (details in Table II). It is noted that different signal realizations of wind and wave are employed per simulation. Each signal is mean corrected and normalized based on the sample's standard deviation.

C. Effects of varying MWS, SWH and damages on FOWT's dynamics

The effects of four different MWSs on the FOWT's dynamics, are presented through a comparison of PSDs in Fig. 2(a). It is evident that MWSs below 16 m/s lead to a change in the dynamics, especially in frequency range [0.4-0.6] Hz. Moreover, Fig. 2(b) shows that the effects of damages of different magnitude and at different locations almost coincide with the healthy state under the same MWS. This means that the considered damages have small effects and it is difficult to be detected. The PSDs are estimated based on the Welch estimator [24] and with the following settings: Window length 400 samples, 0.95% overlap, Hamming window, frequency resolution of 0.025 Hz.

III. DAMAGE DETECTION METHODS

In the present study, damage detection in the fiber rope mooring lines of the OO-STAR floater based FOWT under the varying MWS and SWH is investigated through two STS methods. The main concept of these methods is that selected features represent the healthy structural dynamics under varying ECs in a proper subspace and damage detection is achieved through the check of the current dynamics belonging to the subspace (see Fig. 3). In the MM-AR method, the subspace is described by multiple Auto-Regressive (AR) models whose parameters act as features [23]. In the FMBM, the subspace is described by a single Functional Model (FM) with it's parameters as features [24]. The methods consist of two phases, the baseline phase which is performed based on data from known structural states and varying ECs and the inspection phase which is based on current data while the structure is under an unknown state.

A. Baseline phase

M simulations corresponding to a sample of MWSs are conducted based on the healthy FOWT, with each simulation characterized by a specific MWS w_r. Only MWS is used as it depends on the SWH. The sample covers the range $[w_{min}, w_{max}]$ via the discrete values $w_r \in w_1, w_2, \ldots, w_M$. One response signal is acquired from each simulation and this results to M response signals.

MM-AR method [23]. The healthy FOWT dynamics under distinct MWSs is represented by M (multiple) AR models which are identified based on the M response signals, one model per each signal. A vector $\boldsymbol{\theta}_{o,w_r}$ containing the AR parameters and its covariance matrix $\boldsymbol{\Sigma}_{\boldsymbol{\theta}_{o,w_r}}$ are obtained from each AR(na) model described by the equation [30, pp. 81-83]:

$$y_{w_r}[t] + \sum_{i=1}^{na} a_i \cdot y_{w_r}[t-i] = e_{w_r}[t] \quad (1)$$

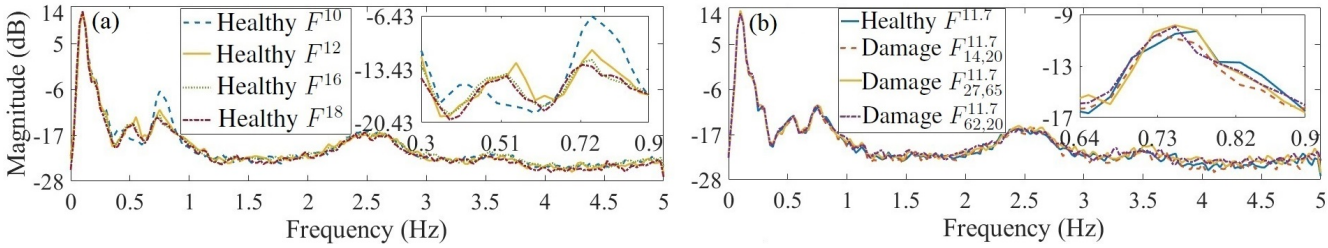

Fig. 2. Comparison of Welch-based PSD estimates using axis z based acceleration signals for (a) the healthy FOWT under seven MWSs and (b) healthy and damage cases under MWS 11.7 m/s

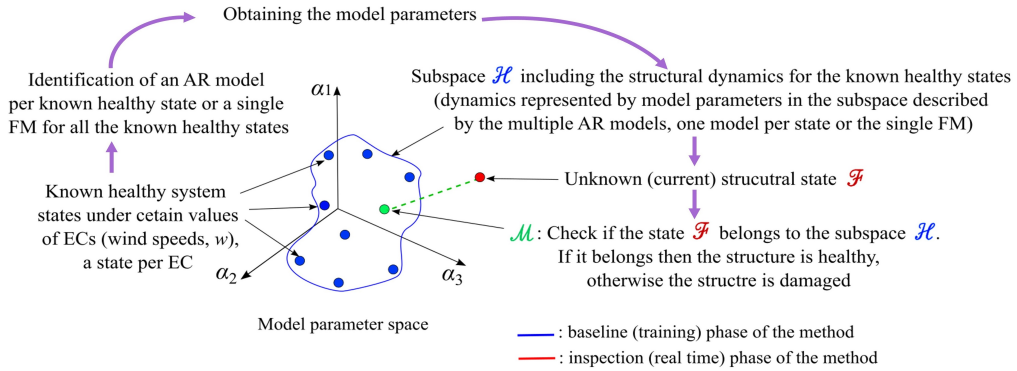

Fig. 3. General concept of damage detection through the methods MM-AR and FMBM

with na designating the AR order, $y_{w_r}[t]$ $(t = 1, \ldots, N)$ the response signal with length of N samples under MWS w_r and $e_{w_r}[t]$ the residual signal that is a white (serially uncorrelated), normally distributed, zero-mean signal with variance $\sigma^2_{e_{w_r}}$. The dimensions of $\boldsymbol{\theta}_{o,w_r}$ and $\boldsymbol{\Sigma}_{\boldsymbol{\theta}_{o,w_r}}$ are $[na \times 1]$ and $[na \times na]$ correspondingly. The AR parameters a_i are estimated through Ordinary Least Squares (OLS) [30, pp. 203-205]. The order of each AR model is determined through the minimization of the Bayesian Information Criterion (BIC) whereas the validation of the models is based on extra set of data not used in the models identification. The validation is achieved through the verification of the uncorrelatedness (whiteness) of the residual signals via standard hypothesis testing [24].

FMBM [24]. The M acquired response signals are used for identifying a single Functionally Pooled AutoRegressive (FP-AR) model [24] (the same M signals used in the **MM-AR method**). An FP-AR$(na)_p$ model is able to describe the healthy dynamics within a continuous range of wind speeds and it is represented by the following equation [24]:

$$y_{w_r}[t] + \sum_{i=1}^{na} a_i(w_r) \cdot y_{w_r}[t-i] = e_{w_r}[t] \tag{2}$$

The AR parameters $a_i(w_r) = \sum_{j=1}^{p} a_{i,j} \cdot G_j(w_r)$, are explicit functions of w_r by belonging to a p-dimensional functional subspace spanned by the (mutually independent) functions $G_1(w_r), G_2(w_r), \ldots, G_p(w_r)$. The functions are orthogonal polynomials of one variable. The $a_{i,j}$ designates the AR projection coefficients. The FP-AR order is selected based on a conventional AR model obtained with a response signal from the healthy FOWT at any MWS. The optimum dimensionality p of the model's functional subspace is selected by minimizing the BIC through a Genetic Algorithm (GA) and the model is validated with extra set of data not used in the FP-AR identification. The validation is achieved through the verification of the whiteness of the model's residual signals via standard hypothesis testing (see **MM-AR method** of Subsect. III-A). In the context of the p selection, the $a_{i,j}$ are estimated through Weighted Least Squares (WLS) [31]. The number and not the type of the used orthogonal polynomials affects the model's ability to describe the dynamics as the families of orthogonal polynomials are essentially equivalent.

B. Inspection phase

MM-AR method [23]. A new AR model is identified based on a new response signal acquired under the FOWT's current (unknown) health state and a new parameter vector $\boldsymbol{\theta}_u$ is obtained. Damage detection is achieved by checking if the current dynamics can be represented by the M baseline AR models and if this is true then the FOWT is in a healthy state (see **MM-AR method** of Subsect. III-A). For this purpose, distance metric H which expresses the distance between the new AR model and the baseline AR models (see **MM-AR method** of Subsect. III-A) is used. This metric is defined as the minimum distance between the current model and the baseline phase models and a damage is detected when H exceeds a user defined limit d_{lim}:

$$\begin{gathered} \text{H} = \min_{r=1,\ldots,M} f(\boldsymbol{\theta}_u, \boldsymbol{\theta}_{o,w_r}) \leq d_{\text{lim}} \Rightarrow \text{healthy FOWT} \\ \text{Else} \Rightarrow \text{damaged FOWT} \end{gathered} \tag{3}$$

with $f(\boldsymbol{\theta}_u, \boldsymbol{\theta}_{o,w_r}) = \sqrt{(\boldsymbol{\theta}_{o,w_r} - \boldsymbol{\theta}_u)^T \cdot \boldsymbol{\Sigma}^{-1}_{\boldsymbol{\theta}_{o,w_r}} \cdot (\boldsymbol{\theta}_{o,w_r} - \boldsymbol{\theta}_u)}$ the Mahalanobis distance between $\boldsymbol{\theta}_u$ and the parameter vector $\boldsymbol{\theta}_{o,w_r}$. The vectors $\boldsymbol{\theta}_u$ and $\boldsymbol{\theta}_{o,w_r}$ must have the same length. The covariance matrix $\boldsymbol{\Sigma}_{\boldsymbol{\theta}_{o,w_r}}$ is used in the Mahalanobis distance as the hypothesis of the FOWT being in a healthy state is made

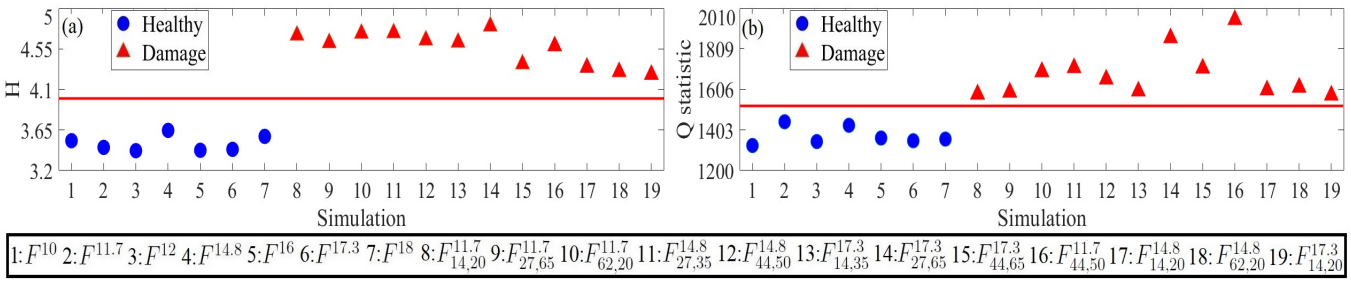

Fig. 4. Damage detection results for (a) the MM-AR method with limit at 4 and (b) the FMBM with limit (—) based on $\alpha = 9 \cdot 10^{-2}$ and $h = 1450$ (bottom box contains the healthy and damage cases corresponding to the simulation numbers)

initially. $\boldsymbol{\theta}_{o,w_r}$ and $\boldsymbol{\Sigma}_{\boldsymbol{\theta}_{o,w_r}}$ are available from the baseline phase (see **MM-AR method** of Subsect. III-A).

FMBM [24]. A new response $y_u[t]$ signal under the FOWT's current (unknown) state and the corresponding known / measured MWS w, are used in the FP-AR$(na)_p$ model (from the baseline phase, see **FMBM** of Subsect. III-A) re-parametrized in terms of w and the residual signal $e_u[t, w]$ is obtained [24]:

$$y_u[t] + \sum_{i=1}^{na} a_i(w) \cdot y_u[t-i] = e_u[t, w] \tag{4}$$

Damage detection is achieved by checking if the current dynamics can be represented by the FP-AR model and if this is true then the FOWT is in a healthy state. For this purpose, a statistical hypothesis test,the Portmanteau test [24], checking the uncorrelatedness (whiteness) of e_u is used. This test is based on the normalized autocorrelation function of the residual signal $\rho_{e_u}[\tau]$ ($\tau = 1, 2, \ldots, h$ lags) and a damage is detected when the hypothesis H_1 and the non-whiteness of the residual signal are accepted:

$$Q \leq \chi^2_{1-\alpha,h} \Rightarrow H_0\text{: } \rho_{e_u}[\tau]=0 \text{ accepted (white residual)} \Rightarrow \text{healthy FOWT} \tag{5}$$

$$\text{Else} \Rightarrow H_1\text{: } \rho_{e_u}[\tau]\neq 0 \text{ accepted (not white residual)} \Rightarrow \text{damaged FOWT}$$

with $Q = N(N+2) \cdot \sum_{\tau=1}^{h} (N-\tau)^{-1} \rho^2_{e_u}[\tau]$.

C. Remarks on the two methods

The MM-AR method necessitates the identification of multiple AR models whereas the FMBM requires a single FP-AR model, with the following consequences:

- An AR model is characterized by simplicity and low structural complexity. Although the estimation of the parameters for multiple AR models in the baseline phase doesn't require much memory, it leads to an increased computation time. The same happens in the inspection phase where multiple parameter comparisons are required for damage detection.
- The FP-AR model's structure is more complex and a higher user expertize for handling the model. Additionally, more memory is required for the AR parameter estimation and the determination of the functional subspace for one FP-AR model in the baseline phase. However, the procedures of estimation and determination are less time costly and the inspection phase also involves a single test.
- The structural dynamics is described under distinct MWSs via the multiple AR models and within a continuous MWS range via the single FP-AR model. Thus, the FP-AR model describes the dynamics under any MWS in the range.

The methods' effectiveness can be improved by using more MWSs from the considered range in the baseline phase.

IV. DAMAGE DETECTION RESULTS

A. Baseline phase

MM-AR method. Seven AR(260) models are identified (*Matlab function: arx.m*) using seven acceleration signals acquired during $M = 7$ simulations with the healthy FOWT and under different MWSs, one model per signal (see Table II). The considered MWSs cover the range $w_r \in [10-18]$ m/s through the discrete values $w_r \in [10, 11.7, 12, 14.8, 16, 17.3, 18]$ m/s. Then, the parameter vector and its covariance matrix are estimated for each AR model. The details of the identified AR models are presented in Table III.

TABLE III
BASELINE PHASE DETAILS OF THE DAMAGE DETECTION METHODS

Detection method	Identified model	No.of simul.	No.of models	Computation time (min)	Memory (MB)
MM-AR	AR(260)	$M=7$	7	9.94	8.6
FMBM	FP-AR$(260)_6$		1	3.29	176.82
Estimation method: OLS (AR), WLS (FP-AR)					
BIC:-2.89 to -3.02 (AR),-20.95 (FP-AR)					
Condition number: $5.53 \cdot 10^3$ to $6.53 \cdot 10^3$ (AR),$1.9 \cdot 10^{11}$ (FP-AR)					
Selecting FP-AR's functional subspace via GA: max generations = 5 (*Matlab function: ga.m*), objective function's tolerance = 10^{-6}					

FMBM. A response signal from the healthy FOWT under MWS 17.3 m/s is used for the identification of an AR model of order $na = 260$. This order is adopted during the identification of an FP-AR model using seven response signals from the healthy FOWT (the same seven signals used in the **MM-AR method**). $p = 6$ univariate Shifted Legendre polynomials consist the selected functional subspace. Thus, the FP-AR$(260)_6$ model is able to represent the healthy FOWT dynamics under any MWS in the range [10-18] m/s. Table III presents the details about the FP-AR model.

B. Inspection phase

MM-AR method / FMBM. Seven healthy cases and twelve damage cases (see Table II) are used for the examination of damage detection. Fig. 4 (a) presents detection results in terms of H metric for the MM-AR whereas Fig. 4 (b) presents

results in terms of Q statistic for the FMBM. Based on these results, it is obvious that all examined healthy and damage cases are detected correctly by both of the methods. The MM-AR requires a computation time of 1.4 min and a memory of 3.71 MB for detection per case and the FMBM 0.13 sec and 101.12 MB correspondingly.

V. CONCLUSIONS

Damage detection in the fiber rope mooring lines of semi-submersible floater based FOWTs has been investigated for the first time in the present study. In particular, the OO-STAR floater based FOWT has been considered. The MM-AR method and the FMBM have been used for damage detection, with the MM-AR employing multiple AR models and being more time costly but less memory consuming and less complex in comparison to the FMBM which employs a single FP-AR model. Although fiber ropes with non-linear behaviour and damages with small effects on the FOWT's dynamics have been implemented in the simulations, the detection results corresponding to healthy and damage cases under varying MWS and SWH have shown that the two employed methods are able to achieve damage detection in the fiber rope mooring lines without any false alarm or missed damage. Based on these promising results, damage detection and quantification for additional damage magnitudes and other varying ECs is under investigation.

ACKNOWLEDGMENT

This research work has been funded by the Research Council of Norway (RCN) through the project "Analytics for asset Integrity Management of Windfarms (AIMWind)", a collaboration between University of Agder, Norwegian Research Center-NORCE AS and Technical University Delft, grant no. 312486. Origo Solutions is included as advisory partner. Access to the design of the OO-STAR wind floater has been granted by it's current owner Bouygues Travaux Publics. The development of the FEM of the OO-STAR floater based FOWT has been funded by the RCN though the project "Fibre Rope Mooring", grant. no 296732.

REFERENCES

[1] R. James and M. C. Ros, "Floating offshore wind: Market and technology review," Carbon Trust, Tech. Rep., 2015.

[2] R. Yang, X. Zheng, J. Chen, and Y. Wu, "Current status and future trends for mooring systems of floating offshore wind turbines," *Sustainable Marine Structures*, vol. 4, pp. 40–54, 2022.

[3] S. D. Weller, L. Johanning, P. Davies, and S. J. Banfield, "Synthetic mooring ropes for marine renewable energy applications," *Renewable Energy*, vol. 83, pp. 1268–1278, 2015.

[4] K. Ma, Y. Wu, S. F. Stolen, L. Bello, M. Horst, and Y. Luo, "Mooring designs for floating offshore wind turbines leveraging experience from the oil & gas industry," in *Proc. 40th International Conference on Ocean, Offshore and Arctic Engineering (OMAE)*, no. 60739, 2021.

[5] Quest Floating Wind Energy, "Floating wind energy: Projects of the world 2022," 2022, https://questfwe.com/map-download-contact-form/.

[6] Principle Power projects, "WindFloat Atlantic and Kincardine FOWT farms," 2022, www.principlepower.com/projects.

[7] H. Dagher, A. Viselli, A. Goupee, R. Kimball, and C. Allen, "The VolturnUS 1:8 floating wind turbine: Design, construction, deployment, testing, retrieval, and inspection of the first grid-connected offshore wind turbine in US," University of Maine, Tech. Rep. DOE-UMaine-3278-2, 2017.

[8] BW Ideol, "Floatgen platform," 2022, https://www.bw-ideol.com/en/floatgen-demonstrator.

[9] Eolink, "Eolink wind turbine - first prototype," 2022, www.eolink.fr/en/article-fp-en.

[10] Saitec, "DemoSATH demonstration project," 2022, www.saitec-offshore.com/en/projects/demosath/.

[11] Stiesdal, "The TetraSpar full-scale demonstration project," 2022, www.stiesdal.com/offshore/the-tetraspar-full-scale-demonstration-project/.

[12] Global Times, "World's first typhoon-resistant floating offshore wind turbine successfully connects to the grid in China," 2021, www.globaltimes.cn/page/202112/1240933.shtml.

[13] Marine Energy Test Centre - Metcentre, "TetraSpar demonstrator," 2022, www.metcentre.no/project/tetraspar-demonstrator-2021/.

[14] R. Sayles, "Spanish group to start building 'disruptive' floating demo," 2020, www.reutersevents.com/renewables/wind/spanish-group-start-building-disruptive-floating-demo.

[15] W. Yu and K. Muller and F. Lemmer, "LIFES50+ D4.2: Public definition of the two LIFES50+ 10MW floater concepts," University of Stuttgart, Tech. Rep., 2018.

[16] H. S. Andersen, E. Dufseth, J. G. Straume, M. H. Madsen, L. Laukeland, and T. Landbo, "Flagship D1.2: D1.2 concept description report," Dr.techn. Olav Olsen, Tech. Rep., 2021.

[17] The Explorer, "Floating offshore wind turbines - OO-Star Wind Floater," 2022, www.theexplorer.no/solutions/offshore-floating-wind-turbines/.

[18] N. Gorostidi, V. Nava, A. Aristondos, and D. Pardo, "Predictive maintenance of floating offshore wind turbine mooring lines using deep neural networks," *Journal of Physics: Conference Series*, vol. 2257, no. 012008, 2022.

[19] Y. Liu, R. Ferrari, P. Wu, X. Jiang, S. Li, and J. W. V. Wingerden, "Fault diagnosis of the 10MW floating offshore wind turbine benchmark: A mixed model and signal-based approach," *Renewable Energy*, vol. 164, pp. 391–406, 2021.

[20] M. Motallebi, H. Ghassemi, and M. Shokouhian, "Deepcwind semi-submersible floating offshore wind turbine platform with a nonlinear multi-segment catenary mooring line and intermediate buoy," *Scientific Journals of the Maritime University of Szczecin*, vol. 69, 2022.

[21] J. Azcona and F. Vittori, "Mooring system design for the 10MW triple spar floating wind turbine at a 180 m sea depth location," *Journal of Physics: Conference Series*, vol. 1356, no. 012003, 2019.

[22] F. Amann, F. Lemmer, M. Borg, S. Raach, D. Schlipf, and H. Bredmose, "Definition of the SWE-TripleSpar floating platform for the DTU 10MW reference wind turbine," University of Stuttgart, Tech. Rep., 2020.

[23] K. J. S. Vamvoudakis, J. S. Sakellariou, and S. D. Fassois, "Vibration based damage detection for a population of nominally identical structures unsupervised multiple model (mm) statistical time series type methods," *Mechanical Systems & Signal Processing*, vol. 111, pp. 149–171, 2018.

[24] C. S. Sakaris, Y. Yang, M. Bashir, C. Michailides, J. Wang, J. S. Sakellariou, and C. Li, "Structural health monitoring of tendons in a multibody floating offshore wind turbine under varying environmental and operating conditions," *Renewable Energy*, vol. 179, pp. 1897–1914, 2021.

[25] T. Landbo, "OO-STAR wind floater the future of offshore wind?" in *Proc. 15th Deep Sea Offshore Wind R&D (DeepWind) conference*, Trondheim, Norway, 2018.

[26] T. Nygaard, J. Vaal, F. Pierella, L. Oggiano, and R. Stenbro, "Development, verification and validation of 3dfloat; aero-servo-hydro-elastic computations of offshore structures," *Energy Procedia*, vol. 94, pp. 425–433, 2016.

[27] C. Felippa and B. Haugen, "A unified formulation of small-strain corotational finite elements: I. theory," *Computer Methods in Applied Mechanics and Engineering*, vol. 194, pp. 2285–2335, 2005.

[28] J. M. Jonkman and L. Kilcher, "TurbSim user's guide: Version 1.06.00," National Renewable Energy Laboratory, U.S. Department of Energy Office of Energy Efficiency & Renewable Energy, Tech. Rep. NREL/TP-xxx-xxxx, 2012.

[29] S. K. Chakrabarti, *Handbook of offshore engineering*. Elsevier, 2005.

[30] L. Ljung, *System identification: Theory for the user*, 2nd ed. Prentice Hall, 1999.

[31] J. S. Sakellariou and S. D. Fassois, "Functionally pooled models for the global identification of stochastic systems under different pseudo-static operating conditions," *Mechanical Systems and Signal Processing*, vol. 72-73, pp. 785–807, 2016.